Published in final edited form as:

Immunity. 2019 June 18; 50(6): 1381–1390.e5. doi:10.1016/j.immuni.2019.04.009.

Cytomegalovirus infection drives avidity selection of natural killer cells

Nicholas M. Adams[1,2], **Clair D. Geary**[1], **Endi K. Santosa**[1], **Dianne Lumaquin**[1], **Jean-Benoît Le Luduec**[1], **Rosa Sottile**[1], **Kattria van der Ploeg**[1], **Joy Hsu**[1], **Benjamin M. Whitlock**[1], **Benjamin T. Jackson**[1], **Orr-El Weizman**[1], **Morgan Huse**[1], **Katharine C. Hsu**[1,3,4], and **Joseph C. Sun**[1,2,5,6,*]

[1]Immunology Program, Memorial Sloan Kettering Cancer Center, New York, NY 10065, USA

[2]Louis V. Gerstner, Jr. Graduate School of Biomedical Sciences, Memorial Sloan Kettering Cancer Center, New York, NY 10065, USA

[3]Department of Medicine, Memorial Sloan Kettering Cancer Center, New York, NY 10065, USA

[4]Department of Medicine, Weill Cornell Medical College, New York, NY 10065, USA

[5]Department of Immunology and Microbial Pathogenesis, Weill Cornell Medical College, New York, NY 10065, USA

[6]Lead Contact

Summary

The process of affinity maturation, whereby T and B cells bearing antigen receptors with optimal affinity to the relevant antigen undergo preferential expansion, is a key feature of adaptive immunity. Natural killer (NK) cells are innate lymphocytes capable of “adaptive” responses following cytomegalovirus (CMV) infection. However, whether NK cells are similarly selected on the basis of their avidity for cognate ligand is unknown. Here, we showed that NK cells with the highest avidity for the mouse CMV glycoprotein m157 were preferentially selected to expand and comprise the memory NK cell pool, whereas low avidity NK cells possessed greater capacity for interferon (IFN)-γ production. Moreover, we provide evidence for avidity selection occurring in human NK cells during human CMV infection. These results delineate how heterogeneity in NK cell avidity diversifies NK cell effector function during antiviral immunity, and how avidity selection may serve to produce the most potent memory NK cells.

[*]Correspondence: Joseph C. Sun, PhD, Memorial Sloan Kettering Cancer Center, 408 East 69th Street, ZRC-1462, New York, NY 10065, Phone: 646-888-3228, Fax: 646-422-0452, sunj@mskcc.org.

Author Contributions

N.M.A. and J.C.S. designed the study. N.M.A., C.D.G., D.L., J.H., B.T.J., and O.E.W performed experiments and collected data. N.M.A. and E.K.S. analyzed the data. B.M.W. and M.H. performed Ca^{2+} imaging of NK cells. J.B.L., R.S., K.P., and K.C.H. collected and analyzed human samples. N.M.A. and J.C.S. wrote the manuscript.

Declaration of Interests

The authors declare no competing interests.

Graphical Abstract

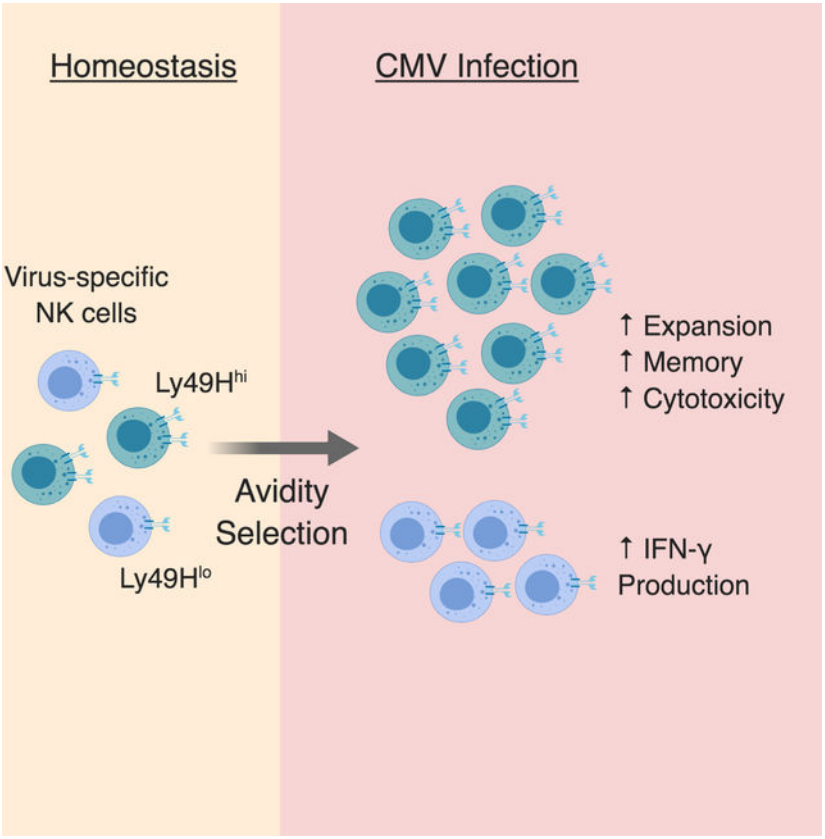

eTOC Blurb

NK cells are innate lymphocytes capable of “adaptive” responses following infection, but whether they undergo avidity selection is unknown. Adams et al. report that diversity in antigen receptor Ly49H expression drives NK cell functional heterogeneity during MCMV infection, with high avidity NK cells being selected to dominate the adaptive response.

Keywords

NK cells; viral infection; cytomegalovirus; heterogeneity; selection

Introduction

A fundamental feature of adaptive immunity is its specificity for a nearly infinite array of potential antigens (Goldrath and Bevan, 1999). During an infectious challenge, the repertoire of presented antigens and competition for these antigens shape the diversity of the effector lymphocyte population in a manner dependent on lymphocyte responsiveness to a given epitope (Johnson et al., 2016; Kedl et al., 2003; Kedl et al., 2000; Oberle et al., 2016). During a primary immune response, competition for antigen and resources results in outgrowth of $CD8^+$ T cells bearing TCRs that recognize their cognate antigen with optimal affinity (Day et al., 2007; Trautmann et al., 2005). B cells iteratively mutate their BCR in the

germinal center via somatic hypermutation until their BCR affinity is optimal for sensing antigen presented by follicular dendritic cells (FDCs), which provide high affinity B cells with necessary survival and proliferation signals, a process known as affinity maturation (Kim et al., 1981; Küppers et al., 1993; MacLennan, 1994; Muramatsu et al., 1999). Furthermore, T cell affinity maturation occurs during a secondary or recall response, a selective process in which the diversity of the epitopespecific $CD8^+$ T cell TCR repertoire becomes restricted (Busch and Pamer, 1999). Thus, the adaptive immune system evolves in real-time by selecting lymphocytes best able to combat the specific pathogens encountered.

Natural killer (NK) cells are innate lymphocytes that play a critical, dominant role in herpesvirus control in both mice and humans (Biron et al., 1989; Bukowski et al., 1985; Etzioni et al., 2005). Although traditionally categorized under innate immunity, NK cells can exhibit “adaptive” antiviral responses to mouse cytomegalovirus (MCMV), including robust clonal proliferation and establishment of a long-lived population of memory cells with enhanced functionality and protective capacity following MCMV reinfection (Sun et al., 2009). In C57BL/6 mice, a subset of naïve NK cells bearing the activating receptor Ly49H undergo this adaptive response following recognition of MCMV-encoded m157, an MHC class I-like glycoprotein expressed on the infected cell surface (Arase et al., 2002; Daniels et al., 2001; Dokun et al., 2001; Sun et al., 2009). In both mice and humans, the combination of stocastically-expressed germline-encoded activating and inhibitory receptors generates NK cell diversity and heterogeneity at the population level (Horowitz et al., 2013; Lanier, 2005). Several groups have reported that heterogeneity within the naïve $Ly49H^+$ NK cell pool affects the antiviral NK cell response, in particular the preferential expansion of unlicensed NK cells, NK cells with a history of recombination-activating gene (RAG) expression, and NK cells that lack expression of killer cell lectin-like receptor G1 (KLRG1) or the inhibitory receptor NKR-P1B (Kamimura and Lanier, 2015; Karo et al., 2014; Orr et al., 2010; Rahim et al., 2016). However, whether $Ly49H^+$ NK cells undergo selection during generation of the effector and memory pool on the basis of their avidity for m157 remains unresolved. Here, we interrogated the effect that heterogeneity in antigen receptor expression has on $Ly49H^+$ NK cell functional responses, and provide evidence that both mouse and human NK cells undergo avidity selection during CMV infection.

Results

MCMV m157 drives higher Ly49H expression within the antiviral NK cell pool

To investigate whether viral infection modulates the avidity of the virus-specific NK cell pool, we infected wild-type (WT) mice with MCMV and observed increased surface expression of Ly49H on $Ly49H^+$ NK cells (Figures 1A and S1A). To track antigen-experienced NK cells longitudinally, we transferred $Ly49H^+$ NK cells into Ly49H-deficient recipients ($Klra8^{-/-}$ mice) (Figure 1B). As the endogenous NK cells in $Klra8^{-/-}$ mice cannot engage MCMV m157 (Fodil-Cornu et al., 2008), only the transferred $Ly49H^+$ NK cells undergo MCMV-driven clonal proliferation (Sun et al., 2009). Compared with the naïve $Ly49H^+$ NK pool, effector and memory $Ly49H^+$ NK cells displayed higher Ly49H expression (Figure 1C). In contrast, expression of NK1.1, which recognizes MCMV m12 (Aguilar et al., 2017), remained unchanged on memory NK cells (Figure 1D), indicating that

the sustained change in the distribution of Ly49H expression on MCMV-driven NK cells may be unique among NK cell activating receptors. Neither infection with MCMV lacking m157 (MCMV-*Δm157*) nor with *Listeria monocytogenes* affected Ly49H expression on Ly49H$^+$ NK cells (Figure 1E), indicating that m157 is required for this process. During MCMV infection, NK cells are exposed not only to m157 on infected cells, but also to an environment rich in proinflammatory cytokines (Biron and Tarrio, 2015). However, NK cells unresponsive to interleukin (IL)-12 (*Stat4*$^{-/-}$), IL-18 (*Il18r1*$^{-/-}$), and type I interferon (IFN) (*Ifnar1*$^{-/-}$ and *Stat1*$^{-/-}$) expressed Ly49H comparably to WT effector NK cells following MCMV infection (Figures 1F and S1B), suggesting that these cytokines are individually dispensable for the MCMV-driven avidity changes. Thus, MCMV infection elicits an m157-dependent change in the distribution of Ly49H expression on effector and memory Ly49H$^+$ NK cells.

Avidity selection shapes the effector and memory NK cell pool during MCMV infection

We reasoned that one explanation for a population increase in Ly49H could be preferential expansion of Ly49H$^+$ NK cells with greater baseline Ly49H expression (i.e. avidity selection). To test this hypothesis, we purified equal numbers of Ly49H$^+$ NK cells with different Ly49H receptor abundance (Ly49H^{lo} and Ly49H^{hi}, defined as Ly49H$^+$ NK cells in the bottom or top ~20% of Ly49H median fluorescence intensity (MFI), respectively) from congenically distinct WT mice, co-transferred them into MCMV-infected Ly49H-deficient recipients, and longitudinally analyzed their activation and expansion (Figures 2A and S1C). Although both Ly49H^{lo} and Ly49H^{hi} NK cells clonally expanded and formed memory (Figures 2B and 2C), the magnitude of their responses differed, regardless of their congenic markers (Figure S2A). Ly49H^{hi} NK cells expanded more robustly and outnumbered Ly49H^{lo} NK cells at 7 days post infection (PI) (the peak of the antiviral response) and preferentially contributed to the memory NK cell pool in peripheral blood and various tissues at 28 days PI (Figures 2B and 2C). The ratio of Ly49H^{hi} to Ly49H^{lo} NK cells did not diverge further during contraction (Figure 2C), suggesting the greater abundance of Ly49H^{hi} memory NK cells is due to their expansion advantage. Even in a non-competitive setting, when Ly49H^{lo} and Ly49H^{hi} NK cells were transferred into separate animals, Ly49H^{hi} NK cells produced a larger effector and memory population (Figure S2B), indicating that NK cell avidity for viral ligand regulates intrinsic aspects of the antiviral NK cell response. Despite their differential expansion, Ly49H^{lo} and Ly49H^{hi} NK cells matured similarly (Figure S2C). They also retained their relative differences in Ly49H expression following infection (Figure 2D), suggesting that Ly49H expression is clonally maintained. Naïve NK cells co-expressing both Ly49H and Ly49D exhibited reduced abundance of each receptor compared to naïve NK cells expressing either Ly49H or Ly49D alone (Figure S2D). Thus, Ly49D expression may contribute to establishing heterogeneity in Ly49H expression within the naïve NK cell pool.

We also evaluated whether avidity maturation (i.e. upregulation of Ly49H within an individual NK cell) and avidity selection occur concomitantly. Ly49H^{lo} NK cells increased their expression of Ly49H, most notably during the contraction phase, with Ly49H expression increasing 2- to 3-fold compared to that of naïve Ly49H^{lo} NK cells (Figure S2E). In contrast, MCMV-driven Ly49H^{hi} NK cells did not considerably increase their Ly49H

expression relative to naïve Ly49H^{hi} NK cells (Figure S2E), suggesting there may be an "upper limit" for Ly49H expression on NK cells.

To investigate the mechanism behind differential expansion of Ly49H^{lo} and Ly49H^{hi} NK cells, we transferred bulk splenocytes labeled with Cell Trace Violet (CTV) into WT mice. Following MCMV infection, Ly49H^{hi} NK cells divided more efficiently (Figure 2E). Furthermore, during MCMV-driven expansion, Ly49H^{hi} NK cells demonstrated lower caspase activity as assessed by fluorescent labeled inhibitors of caspases (FLICA) staining (Figure 2F). Collectively, these data suggest that NK cell avidity regulates the proliferative capacity and survival of a given Ly49H^{+} NK cell during MCMV infection, which underlies the greater expansion and subsequent memory pool establishment of Ly49H^{hi} NK cells.

NK cell avidity regulates m157-mediated activation and cytotoxicity

These data raised the possibility that Ly49H density affects NK cell engagement with infected cells (i.e. avidity) or the magnitude of Ly49H-dependent signaling. To test this, we performed live cell imaging of Ly49H^{lo} and Ly49H^{hi} NK cells co-cultured with Ba/F3 cells expressing m157 (Ba/F3–m157). Ly49H receptor ligation results in phosphorylation of its adaptor DAP12, which recruits and activates Syk and zeta chain of T cell receptor associated protein kinase 70 (ZAP70), initiating their signaling cascades and resulting in increased intracellular calcium (Lanier, 2008). To visualize productive target cell encounters that resulted in activation-induced Ca^{2+} flux, NK cells were labeled with the cell permeable Fura-2 calcium indicator. Ly49H^{hi} NK cells made more contacts with Ba/F3–m157 cells than did Ly49H^{lo} NK cells, and a greater percentage of Ly49H^{hi} NK cell contacts resulted in NK cell activation and Ca^{2+} flux (Figure 2G). These results suggest that Ly49H^{hi} NK cells may be preferentially recruited into the antiviral response.

Given that NK cell cytotoxicity requires activating receptor engagement, we speculated that NK cell cytotoxic function is dependent on avidity for cognate ligand. To assess this, we separately co-cultured Ly49H^{-}, Ly49H^{lo}, and Ly49H^{hi} NK cells with equal numbers of target Ba/F3–m157 and control Ba/F3 cells labeled differentially with CTV. Although Ly49H^{lo} cells were capable of killing Ba/F3–m157 target cells, Ly49H^{hi} cells possessed the most potent cytotoxic function (Figures 2H, S2F and S2G). The enhanced functionality of Ly49H^{hi} NK cells was strictly Ly49H-dependent, as a greater percentage of Ly49H^{hi} NK cells produced IFN-γ and degranulated only in response to Ly49H ligation *ex vivo*, but not NK1.1 ligation or phorbol 12- myristate 13-acetate (PMA) and ionomycin (Figure S2H), excluding a developmentally-determined general heightened reactivity of these cells. Collectively, these data indicate that higher Ly49H expression precipitates greater Ly49H-dependent activation and effector function (i.e. functional avidity) in the presence of target cells expressing cognate ligand.

Ly49H density specifies differential effector functions of Ly49H^{+} NK cells during early MCMV infection

The detection of viral ligand-bearing infected cells by Ly49H^{+} NK cells is an essential signal for NK cell-mediated host protection, yet MCMV also induces a highly inflammatory environment rich in IL-12, IL-18, and type I interferon (Biron and Tarrio, 2015). These

cytokines can lead to nonspecific activation of NK cells, promote NK cell effector function (e.g. IFN-γ production), and program their adaptive responses (Biron and Tarrio, 2015; Dokun et al., 2001; Madera et al., 2016; Madera and Sun, 2015; Sun et al., 2012). To comprehensively understand how avidity regulates the NK cell response to MCMV, we performed RNA-seq on splenic Ly49H^{lo} and Ly49H^{hi} NK cells during early MCMV infection (day 1.5 PI). Of the 1941 differentially expressed genes ($p_{adj} < 0.05$), 1232 transcripts were upregulated and 709 downregulated in Ly49H^{hi} NK cells (Table S1), the top 100 of which are shown in Figure 3A. KEGG pathway analysis of differentially expressed genes revealed an enrichment of cell cycle control, DNA replication, and genome integrity maintenance genes in Ly49H^{hi} NK cells (Figures 3B and S3A), consistent with their proliferative advantage (Figure 2E). In contrast, genes upregulated in Ly49H^{lo} NK cells were primarily involved with cytokine and JAK-STAT signaling (Figures 3C and S3B). The extent and nature of the transcriptional differences underscore the diversity within the Ly49H^{+} NK cell compartment and the divergence of their cellular activities within the earliest days of infection.

To validate and extend our RNA-seq results, we focused on several differentially expressed genes notable for their role in NK cells and regulation by proinflammatory cytokines. Transcript (*Il2ra*) and protein (CD25) of the high-affinity α subunit of the IL-2 receptor were both more robustly upregulated in Ly49H^{lo} NK cells during MCMV infection (Figures S3C and S3D). Furthermore, consistent with higher quantities of *Ifng* (encoding IFN-γ) transcripts in Ly49H^{lo} NK cells (Figure 3D), a greater percentage of Ly49H^{lo} NK cells produced IFN-γ during MCMV infection (Figure 3E), and Ly49H^{lo} NK cells produced more IFN-γ than Ly49H^{hi} NK cells on a per-cell basis (Figure S3E). In *Ifng*-IRES-YFP reporter mice ("GREAT" mice), Ly49H^{lo} NK cells more robustly upregulated *Ifng* transcript during MCMV infection (Figure 3F). However, prior to infection, there were no differences in baseline *Ifng* transcript (Figures 3F and S3F) or their ability to produce IFN-γ following IL-12 and IL-18 stimulation *ex vivo* (Figure S2H), suggesting that infection-specific differences in the regulation of the *Ifng* locus accounted for the observed phenotype. Although bulk Ly49H^{-} and Ly49H^{+} NK cells are thought to express similar IFN-γ at this early time point (Dokun et al., 2001), the "population average" across Ly49H^{+} NK cells concealed considerable heterogeneity in the Ly49H^{+} NK cell compartment (Figure S3G). Thus, the extent of Ly49H signaling *in vivo* during MCMV infection regulates NK cell effector properties.

Ly49H^{lo} and Ly49H^{hi} NK cells had similar maturation profiles (by CD11b and CD27 subsets) despite modest differences in KLRG1 (Figure S3H), and similar proportions of both NK cell populations expressed NKG2A (Figure S3I), one of the inhibitory receptors licensed in C57BL/6 mice. A greater proportion of Ly49H^{hi} NK cells expressed Ly49C/I (Figure S3I), yet consistent with an earlier report (Orr et al., 2010), Ly49C/I expression did not effect IFN-γ production *in vivo* during MCMV infection (Figure S3J). Thus, the functional and transcriptional differences between Ly49H^{lo} and Ly49H^{hi} NK cells during MCMV infection are likely due to infection-specific, rather than developmental differences. Furthermore, Ly49H^{lo} and Ly49H^{hi} NK cells displayed similar abundance of phosphorylated STAT4 (pSTAT4), comparable IL-18 receptor alpha (IL-18Ra), and transcripts encoding IL-12 receptor chains (Figures S3K and S3L). Thus, Ly49H-mediated regulation of

proinflammatory cytokine responsiveness is likely occurring further downstream of cytokine receptor expression and STAT4 phosphorylation.

To understand whether the functional differences between these two NK cell subsets have a physiological role in host defense, we compared protection of susceptible *Rag2*$^{-/-}$ *Il2rg*$^{-/-}$ mice by Ly49H^{lo} or Ly49H^{hi} NK cells. Although Ly49H^{lo} NK cells provided some protection against MCMV (compared to mice that did not receive NK cells), Ly49H^{hi} NK cells significantly extended the survival of susceptible hosts beyond that of Ly49H^{lo} NK cells (Figure 3G). Collectively, these results reveal that the avidity-dependent functional differences between Ly49H^{lo} and Ly49H^{hi} NK cells regulate the protective antiviral responses mounted by NK cells.

Human NK cells show evidence for avidity selection during HCMV infection

Analogous to the Ly49H^{+} NK cell response against MCMV in mice, CD94/NKG2C^{+} NK cells are expanded in the peripheral blood of human cytomegalovirus (HCMV)-seropositive healthy individuals (Gumá et al., 2004; Lopez-Vergès et al., 2011), as well as in recipients of solid organ and hematopoietic stem cell transplants (HSCT) who reactivate HCMV (Della Chiesa et al., 2012; Foley et al., 2012; Horowitz et al., 2015; Lopez-Vergès et al., 2011; Muccio et al., 2016). HCMV-encoded UL40 peptides loaded onto HLA-E were recently shown to activate human NKG2C^{+} NK cells in a peptide-specific manner (Hammer et al., 2018), comparable to the interaction between MCMV m157 and Ly49H in mice. To determine whether HCMV infection similarly modulates the avidity of human NKG2C^{+} NK cells, we analyzed NK cells from peripheral blood of T cell-depleted HSCT recipients. In the transplant setting, the timing of HCMV infection (or reactivation in patients previously reported to be HCMV-seropositive) can be estimated, which enabled longitudinal analysis of NK cells in the same patient. Consistent with previous reports (Foley et al., 2012; Horowitz et al., 2015; Muccio et al., 2016), NKG2C^{+} NK cells were expanded in HSCT patients following HCMV detection (Figure 4A). Phenotypic analysis revealed higher NKG2C expression on the expanded NKG2C^{+} NK cell population from HCMV-reactivating patients, but not on the unexpanded population of NKG2C^{+} NK cells from patients who remained HCMV-seronegative post-transplant (Figure 4B). This evidence supports the notion that NK cell avidity selection during CMV infection may be conserved between mouse and human.

In a larger healthy human cohort, HCMV-seronegative donors had minimal variation in NKG2C expression and NKG2C^{+} NK cell percentage, whereas HCMV-seropositive donors displayed a positive linear relationship between NKG2C expression and percentage of NKG2C^{+} NK cells (Figure 4C). Similarly, during the mouse Ly49H^{+} NK cell response to MCMV, Ly49H expression strongly correlated with expansion of the Ly49H^{+} NK cell population at the peak of the antiviral response (Figure 4D). These data support the idea that the degree of virus-driven NK cell expansion and the extent of NK cell avidity selection are closely linked processes in both mice and humans.

Discussion

Our study provides a mechanistic understanding of how avidity for viral ligand regulates the functional contribution of an NK cell during MCMV infection. Although NK cells of

varying avidities were recruited during early MCMV infection, similar to $CD8^+$ T cells with a range of TCR affinities (Zehn et al., 2009), high avidity NK cells preferentially expanded. Concurrent with our studies using NK cell populations sorted on the basis of Ly49H surface density, Grassmann et al. used retrogenic color barcoding to track single NK cell-derived responses (Grassmann et al., 2019). In accordance with our findings, they also observed that Ly49H expression in individual NK cell clones correlated with the degree of their clonal expansion. Thus, the major conclusions from both of these complementary studies are in agreement. Furthermore, it appeared that effector and memory $Ly49H^{lo}$ NK cells expressed more Ly49H than they do as naïve NK cells, suggesting that avidity maturation (i.e. upregulation of Ly49H within an individual NK cell) and avidity selection may be occurring concomitantly. Together these processes may contribute to the generation of a memory NK cell pool with heightened specificity for MCMV re-encounter (Sun et al., 2009).

Previous *in vivo* imaging studies have described that TCR transgenic $CD8^+$ T cell priming by cognate peptide-loaded DCs occurs in three phases: 1) transient serial encounters with DCs, 2) stable contacts with DCs, and 3) $CD8^+$ T cell motility and proliferation (Mempel et al., 2004). Stable contacts between $CD8^+$ T cells and DCs are required for the full differentiation program. These stronger and longer interactions program $CD8^+$ T cell clonal expansion, and are dependent on the absolute number of TCR-pMHC interactions (Henrickson et al., 2008). Furthermore, high affinity TCR ligands and prolonged antigen exposure dictate the duration and magnitude, respectively, of the $CD8^+$ T cell expansion (Prlic et al., 2006; Zehn et al., 2009). Our data reveal that many requirements for naïve $CD8^+$ T cell and NK cell priming and clonal expansion are conserved. Although MCMV infection activated both $Ly49H^{lo}$ and $Ly49H^{hi}$ NK cells, these cells were transcriptionally distinct during the earliest days of infection. We speculate that the number of activating receptor-cognate ligand interactions regulates the strength or duration of contact between an NK cell and an infected cell, which plays a fundamental role in programming the response of that cell.

Despite the greater potential of $Ly49H^{hi}$ NK cells for expansion and cytotoxicity, $Ly49H^{lo}$ NK cells were the primary IFN-γ-producing NK cells during the early effector response, suggesting a division of labor between these two cell populations. One possibility is that an NK cell must allocate cellular and metabolic resources for the competing demands of IFN-γ secretion and expansion, or that strong Ly49H receptor ligation may antagonize NK cell responsiveness to proinflammatory cytokines. Indeed, MCMV-driven memory NK cells, which have greater Ly49H surface density, have diminished bystander responses to heterologous infection (Min-Oo and Lanier, 2014). Thus, strong Ly49H activation precipitates both immediate and heritable changes in IFN-γ production.

$Ly49H^{lo}$ and $Ly49H^{hi}$ NK cells maintained their relative differences in Ly49H density following MCMV-driven proliferation, suggesting clonal maintenance of Ly49H expression. Given that *Klra8* (encoding Ly49H) was the most differentially expressed gene ranked by p-value between $Ly49H^{lo}$ and $Ly49H^{hi}$ NK cells at day 1.5 PI (Table S1), we hypothesize that Ly49H expression is transcriptionally maintained during infection. Since the effector function profile of an NK cell during MCMV infection hinges on its Ly49H expression, further investigation into the full complement of factors (of which, Ly49D may be one such

variable) that regulate and maintain Ly49H expression during development, homeostasis, and infection is warranted.

Analogous to avidity selection of mouse NK cells during MCMV infection, we demonstrated that the NKG2C$^+$ NK cell pool that arose in HSCT recipients following HCMV infection or reactivation expressed more NKG2C. *NKG2C* zygosity has been reported to influence surface receptor density and NKG2C$^+$ NK cell numbers in HCMV$^+$ subjects (Muntasell et al., 2013), and could contribute to the range in these parameters in our transplant patient cohort that reactivated HCMV. Future work is required to determine the molecular mechanisms behind avidity selection of human NK cells, and how avidity affects human NK cell repertoire diversity based on prior pathogen experience (Strauss-Albee et al., 2015). Nevertheless, our findings collectively indicate that avidity selection may be a general mechanism in NK cell biology conserved between mouse and human, likely resulting from the extensive co-evolution of NK cells with CMV, and can inform vaccination strategies to elicit memory NK cells with the greatest avidity for viral ligands.

STAR Methods

Contact for Reagent and Resource Sharing

Further information and requests for resources and reagents should be directed to and will be fulfilled by the Lead Contact, Joseph Sun (sunj@mskcc.org).

Experimental Model and Subject Details

Mice—All mice used in this study were housed and bred under specific pathogen-free conditions at Memorial Sloan Kettering Cancer Center (MSKCC), and handled in accordance with the guidelines of the Institutional Animal Care and Use Committee (IACUC). The following mouse strains were used in this study: C57BL/6 (CD45.2), B6.SJL (CD45.1), *Klra8*$^{-/-}$ (Ly49H-deficient) (Fodil-Cornu et al., 2008), *Stat4*$^{-/-}$, *Il18r1*$^{-/-}$, *Ifnar1*$^{-/-}$, *Stat1*$^{-/-}$, *Ifng*-IRES-YFP (GREAT), and *Rag2*$^{-/-}$ *Il2rg*$^{-/-}$ mice. Experiments were conducted using age- and gender-matched mice in accordance with approved institutional protocols. Mice used in this study were of both genders and were 6–8 weeks of age at the time of experimentation.

Primary Human Cells—Peripheral blood samples were collected from allogeneic bone marrow transplantation patients and healthy human donors following approval from the MSKCC Institutional Review Board, and donors provided informed, written consent. Peripheral blood mononuclear cells (PBMCs) were isolated by Ficoll centrifugation. Additional PBMCs were isolated from buffy coats obtained from healthy volunteer donors via the New York Blood Center (NYBC, http://nybloodcenter.org/). The MSKCC IRB waived the need for additional research consent for anonymous NYBC samples. Donors were of both genders and ranged in age between 12 and 76 years old. PBMCs were cryopreserved in fetal bovine serum with 10% DMSO. HCMV serostatus was provided by NYBC.

Virus—MCMV (Smith strain) was serially passaged through BALB/c hosts three times, and then salivary gland viral stocks were prepared with a dounce homogenizer for dissociating the salivary glands of infected mice 3 weeks after infection.

Bacteria—Frozen stocks of *Listeria monocytogenes* were grown in brain-heart infusion (BHI) broth. Bacteria culture samples were grown to mid-log phase, measured by optical density (A600), and diluted in PBS for injection.

Method Details

***In Vivo* Virus Infection—**Adoptive co-transfer studies (both competitive and non-competitive) were performed by transferring 10^5 Ly49H^{lo} NK cells and/or 10^5 Ly49H^{hi} NK cells, purified from spleens of congenically distinct WT mice (CD45.1 or CD45.2), into *Klra8*$^{-/-}$ mice 1 day prior to MCMV infection. Recipient mice in adoptive (co-)transfer studies were infected with MCMV by intraperitoneal (i.p.) injection of 7.5×10^2 plaque-forming units (PFU) in 0.5 mL.

Survival studies were performed by transferring either no cells, 5×10^4 purified splenic Ly49H^{lo} NK cells, or 5×10^4 purified splenic Ly49H^{hi} NK cells into *Rag2*$^{-/-}$ *Il2rg*$^{-/-}$ mice 2 days prior to MCMV infection. Recipient mice in survival studies were infected with 7.5×10^3 PFU MCMV in 0.5 mL by i.p. injection.

In several experiments, WT mice were directly infected with MCMV (7.5×10^3 PFU) or MCMV-*Δm157* (10^5 PFU) (Bubic et al., 2004) in 0.5 mL by i.p. injection.

***In Vivo* Bacterial Infection—**Mice were infected with priming doses equivalent to 2000–5000 colony forming units (CFU) by tail vein injection.

Lymphocyte Isolation—Spleens were dissociated using glass slides and filtered through a 100-μm strainer. To isolate lymphocytes from liver, the tissue was physically dissociated using a glass tissue homogenizer and purified using a discontinuous gradient of 40% over 60% Percoll. Red blood cells in blood, spleen, and liver were lysed using ACK lysis buffer.

Flow Cytometry and Cell Sorting—Cell surface staining of single-cell suspensions from various organs was performed using fluorophore-conjugated antibodies (BD Biosciences, eBioscience, BioLegend, Tonbo Biosciences, Beckman Coulter, Miltenyi). Intracellular staining was performed by fixing and permeabilizing with the eBioscience Foxp3 Transcription Factor Staining Set (Thermo Fisher) for staining intranuclear proteins and cytokines, or with formaldehyde and methanol for staining phosphorylated STAT proteins.

Flow cytometry and cell sorting were performed on the LSR II and Aria II cytometers (BD Biosciences), respectively. Data were analyzed with FlowJo software (Tree Star). Flow cytometry of mouse lymphocytes was performed using the following fluorophore-conjugated antibodies: CD3ε (17A2), TCRβ (H57–597), CD19 (6D5), F4/80 (BM8.1), NK1.1 (PK136), Ly49H (3D10), CD45.1 (A20), CD45.2 (104), CD11b (M1/70), CD27 (LG. 7F9), KLRG1 (2F1), Ly49D (4E5), Ly49C/I (5E6), NKG2A/C/E (20D5), CD25 (PC61),

IFN-γ (XMG1.2), CD107a (1D4B), STAT4 pY693 (38/p-Stat4), IL-18Ra (P3TUNYA), and Fixable Viability Dye. Staining of human PBMCs was performed using: CD3 (UCHT1), CD56 (N901), NKG2C (REA205), and LIVE/DEAD as viability marker.

Apoptosis was evaluated by caspase activity staining using the carboxyfluorescein FLICA poly caspase assay kit (Bio-Rad). NK cell proliferation was analyzed by labeling cells with 5 μM CellTrace Violet (CTV, Thermo Fisher) prior to transfer, and CTV labeling was performed according to manufacturer protocol.

NK Cell Enrichment and Purification—NK cells ($TCR\beta^-CD3\varepsilon^-CD19^-F4/80^-CD45^+NK1.1^+$) were enriched from spleens of pooled C57BL/6 mice by negative selection over BioMag goat anti-rat IgG beads (Qiagen) coated with rat anti-mouse CD8α, CD4, CD19, and Ter-119 antibodies (Bio X Cell, clones 2.43, GK1.5, 1D3, and TER-119 respectively) before being sorted to high purity on an Aria II cytometer (BD Biosciences).

***Ex Vivo* Stimulation of Lymphocytes—**10^4 purified splenic $Ly49H^{lo}$ or $Ly49H^{hi}$ NK cells were stimulated for 4 hours in RPMI containing 10% fetal bovine serum with 20 ng/mL recombinant mouse IL-12 (R&D Systems) plus 10 ng/mL IL-18 (MBL), 10 ng/mL PMA (Sigma) plus 1 g/mL Ionomycin (Sigma), or 25 g/mL of plate-bound anti-mouse NK1.1 (PK136, BioLegend) or anti-mouse Ly49H (3D10, BioLegend). Cells were cultured in media alone as a negative control.

Ca^{2+} Imaging of NK Cells—Purified splenic NK cells ($TCR\beta^-CD3\varepsilon^-CD19^-F4/80^-CD45^+NK1.1^+$) with different Ly49H expression were loaded with 5 μg/ml Fura-2AM for 30 min and transferred into colorless RPMI (no phenol red) containing 5% FCS. 8×10^4 NK cells were mixed 1:4 with Ba/F3–m157 cells and imaged in 8-well chamber slides (Thermo Fisher Scientific) using an inverted fluorescence video microscope (IX-81; Olympus) fitted with a 20×, 0.75 NA objective lens (Olympus). A Xe lamp (DG-4; Sutter Instrument) was used for fluorophore excitation, and data were collected on an electron-multiplying charge-coupled device camera (ImagEM; Hamamatsu Photonics). Time-lapse recordings were made using SlideBook software (Intelligent Imaging Innovations). One brightfield image and one Fura-2 image were taken every 20 s for 20 min.

***Ex Vivo* Killing Assay—**Ba/F3 control cells and Ba/F3–m157 target cells (Arase et al., 2002) were labeled differentially with CTV (Ba/F3, CTV^{lo}; Ba/F3–m157, CTV^{hi}). 5×10^3 of each cell line were mixed with 5×10^4 purified splenic NK cells with different Ly49H expression, or without NK cells (control condition). Effector and target cells were co-cultured for 6 hours at 37°C in RPMI-1640 containing 10% FBS. After 6 hours, cells were stained with propidium iodide prior to flow cytometry. The percentages of target cell killing were determined using the following formula, adapted from (Viant et al., 2017): 100 −([(% Ba/F3–m157 cells/% Ba/F3 cells)]/[(% Ba/F3–m157 cells/% Ba/F3 cells) control] × 100). For this formula, only CTV^+ cells within live cells were considered. The percentage of propidium iodide-staining target cells was determined from total CTV^{hi} cells.

RNA Sequencing—Ly49H^{lo} and Ly49H^{hi} NK cells were sorted from the spleens of WT mice 1.5 days post MCMV infection. Spleens from three infected mice were pooled to achieve ~5×10^4 cells of each population (one paired replicate). RNA from cells suspended in Trizol was extracted with chloroform. Isopropanol and linear acrylamide were added, and the RNA was precipitated with 75% ethanol. Samples were resuspended in RNase-free water. After RiboGreen quantification and quality control by Agilent BioAnalyzer, 2ng total RNA with RNA integrity numbers ranging from 8.1 to 10 underwent amplification using the SMART-Seq v4 Ultra Low Input RNA Kit (Clonetech catalog # 63488), with 12 cycles of PCR. Subsequently, 10ng of amplified cDNA were used to prepare libraries with the KAPA Hyper Prep Kit (Kapa Biosystems KK8504) using 8 cycles of PCR. Samples were barcoded and run on a HiSeq 4000 in a 50bp/50bp paired end run, using the HiSeq 3000/4000 SBS Kit (Illumina). An average of 38 million paired reads were generated per sample and the percent of mRNA bases per sample ranged from 79% to 81%.

Quantification and Statistical Analysis

RNA Sequencing Analysis—Paired-end reads were trimmed for adaptors and removal of low-quality reads using Trimmomatic (v.0.36) (Bolger et al., 2014). Trimmed reads were mapped to the *Mus musculus* genome (mm10 assembly) and counted at transcript-level using quasi-mapping approach by Salmon (v0.10.2) (Patro et al., 2017). These transcript-level estimates were then summarized at gene-level using tximport (v1.9.12) (Soneson et al., 2015). Differential expression (DE) analysis was executed with DESeq2 (v1.12.17) (Love et al., 2014) using UCSC knownGene model as a reference annotation. Genes were considered to be differentially expressed between two groups (Ly49H^{hi} versus Ly49H^{lo}) if their adjusted p-values were less than 0.05. Gene Ontology (GO) analysis was performed using goseq (v1.33.0) (Young et al., 2010) on KEGG pathway database (KEGG.db v3.2.3) with a cutoff of $\log_2$ fold change > 0 or < 0 for DE upregulated or downregulated genes, respectively.

Statistical Analysis—For graphs, data are shown as mean ± SEM, and unless otherwise indicated, statistical differences were evaluated using an unpaired, two-tailed Student's t test, assuming equal sample variance. For experiments in which Ly49H^{lo} and Ly49H^{hi} NK cells were compared within the same mouse, a paired, two-tailed t test was used. Statistical differences in survival were determined by the Log-rank (Mantel-Cox) test. $p < 0.05$ was considered significant. Graphs were produced and statistical analyses were performed using GraphPad Prism.

Data Availability

RNA-seq data comparing Ly49H^{lo} and Ly49H^{hi} NK cells during early MCMV infection (day 1.5 PI) are available in the Gene Expression Omnibus (GEO) under accession code GSE129490.

Supplementary Material

Refer to Web version on PubMed Central for supplementary material.

Acknowledgments

We thank members of the Sun lab, Georg Gasteiger, and Christin Friedrich for experimental assistance, and members of the MSKCC NK club for discussions. We thank Lewis Lanier for helpful discussions and comments on the manuscript. We thank Simon Grassmann and Veit Buchholz for sharing their manuscript with us before publication. Graphical abstract was created with created with BioRender. N.M.A., D.L., and B.T.J. were supported by an MSTP grant from the NIGMS of the NIH (T32GM007739 to the Weill Cornell/Rockefeller/Sloan Kettering Tri-Institutional MD-PhD Program). N.M.A. was also supported by an F30 Predoctoral Fellowship from the NIH NIAID (F30 AI136239). M.H. was supported by NIH grant AI087644. K.C.H. was supported by NIH grant AI123658 and CA023766. J.C.S. was supported by the Ludwig Center for Cancer Immunotherapy, the American Cancer Society, the Burroughs Wellcome Fund, and the NIH (AI100874, AI130043, and P30CA008748).

References

Aguilar OA, Berry R, Rahim MM, Reichel JJ, Popović B, Tanaka M, Fu Z, Balaji GR, Lau TN, Tu MM, et al. (2017). A viral immunoevasin controls innate immunity by targeting the prototypical natural killer cell receptor family. Cell 169, 58–71. [PubMed: 28340350]

Arase H, Mocarski ES, Campbell AE, Hill AB, and Lanier LL (2002). Direct recognition of cytomegalovirus by activating and inhibitory NK cell receptors. Science 296, 1323–1326. [PubMed: 11950999]

Biron CA, Byron KS, and Sullivan JL (1989). Severe herpesvirus infections in an adolescent without natural killer cells. N. Engl. J. Med 320, 1731–1735. [PubMed: 2543925]

Biron CA, and Tarrio ML (2015). Immunoregulatory cytokine networks: 60 years of learning from murine cytomegalovirus. Med. Microbiol. Immunol 204, 345–354. [PubMed: 25850988]

Bolger AM, Lohse M, and Usadel B (2014). Trimmomatic: a flexible trimmer for Illumina sequence data. Bioinformatics 30, 2114–2120. [PubMed: 24695404]

Bubic I, Wagner M, Krmpotic A, Saulig T, Kim S, Yokoyama WM, Jonjic S, and Koszinowski UH (2004). Gain of virulence caused by loss of a gene in murine cytomegalovirus. J Virol 78, 7536–7544. [PubMed: 15220428]

Bukowski JF, Warner JF, Dennert G, and Welsh RM (1985). Adoptive transfer studies demonstrating the antiviral effect of natural killer cells in vivo. J. Exp. Med 161, 40–52. [PubMed: 2981954]

Busch DH, and Pamer EG (1999). T cell affinity maturation by selective expansion during infection. J. Exp. Med 189, 701–710. [PubMed: 9989985]

Daniels KA, Devora G, Lai WC, O'Donnell CL, Bennett M, and Welsh RM (2001). Murine cytomegalovirus is regulated by a discrete subset of natural killer cells reactive with monoclonal antibody to Ly49H. J. Exp. Med 194, 29–44. [PubMed: 11435470]

Day EK, Carmichael AJ, ten Berge IJ, Waller EC, Sissons JG, and Wills MR (2007). Rapid CD8+ T cell repertoire focusing and selection of high-affinity clones into memory following primary infection with a persistent human virus: human cytomegalovirus. Journal of immunology 179, 3203–3213.

Della Chiesa M, Falco M, Podestà M, Locatelli F, Moretta L, Frassoni F, and Moretta A (2012). Phenotypic and functional heterogeneity of human NK cells developing after umbilical cord blood transplantation: a role for human cytomegalovirus? Blood 119, 399–410. [PubMed: 22096237]

Dokun AO, Kim S, Smith HR, Kang HS, Chu DT, and Yokoyama WM (2001). Specific and nonspecific NK cell activation during virus infection. Nat. Immunol 2, 951–956. [PubMed: 11550009]

Etzioni A, Eidenschenk C, Katz R, Beck R, Casanova JL, and Pollack S (2005). Fatal varicella associated with selective natural killer cell deficiency. J. Pediatr 146, 423–425. [PubMed: 15756234]

Fodil-Cornu N, Lee SH, Belanger S, Makrigiannis AP, Biron CA, Buller RM, and Vidal SM (2008). Ly49h-deficient C57BL/6 mice: a new mouse cytomegalovirus-susceptible model remains resistant to unrelated pathogens controlled by the NK gene complex. J. Immunol 181, 6394–6405. [PubMed: 18941230]

Foley B, Cooley S, Verneris MR, Pitt M, Curtsinger J, Luo X, Lopez-Vergès S, Lanier LL, Weisdorf D, and Miller JS (2012). Cytomegalovirus reactivation after allogeneic transplantation promotes a

lasting increase in educated NKG2C+ natural killer cells with potent function. Blood 119, 2665–2674. [PubMed: 22180440]

Goldrath AW, and Bevan MJ (1999). Selecting and maintaining a diverse T-cell repertoire. Nature 402, 255–262. [PubMed: 10580495]

Grassmann S, Pachmayr LO, Leube J, Mihatsch L, Andrae I, Flommersfeld S, Oduro J, Cicin-Sain L, Schiemann M, Flossdorf M, and Buchholz VR (2019). Single-cell fate mapping reveals clonal dynamics of adaptive NK-cell responses. Immunity

Gumá M, Angulo A, Vilches C, Gómez-Lozano N, Malats N, and López-Botet M (2004). Imprint of human cytomegalovirus infection on the NK cell receptor repertoire. Blood 104, 3664–3671. [PubMed: 15304389]

Hammer Q, Ruckert T, Borst EM, Dunst J, Haubner A, Durek P, Heinrich F, Gasparoni G, Babic M, Tomic A, et al. (2018). Peptide-specific recognition of human cytomegalovirus strains controls adaptive natural killer cells. Nature immunology 19, 453–463. [PubMed: 29632329]

Henrickson SE, Mempel TR, Mazo IB, Liu B, Artyomov MN, Zheng H, Peixoto A, Flynn MP, Senman B, Junt T, et al. (2008). T cell sensing of antigen dose governs interactive behavior with dendritic cells and sets a threshold for T cell activation. Nat. Immunol 9, 282–291. [PubMed: 18204450]

Horowitz A, Guethlein LA, Nemat-Gorgani N, Norman PJ, Cooley S, Miller JS, and Parham P (2015). Regulation of adaptive NK cells and CD8 T cells by HLA-C correlates with allogeneic hematopoietic cell transplantation and cytomegalovirus reactivation. J. Immunol 195, 4524–4536. [PubMed: 26416275]

Horowitz A, Strauss-Albee DM, Leipold M, Kubo J, Nemat-Gorgani N, Dogan OC, Dekker CL, Mackey S, Maecker H, Swan GE, et al. (2013). Genetic and environmental determinants of human NK cell diversity revealed by mass cytometry. Sci Transl Med 5, 208ra145.

Johnson LR, Weizman OE, Rapp M, Way SS, and Sun JC (2016). Epitope-specific vaccination limits clonal expansion of heterologous naive T cells during viral challenge. Cell Rep 17, 636–644. [PubMed: 27732841]

Kamimura Y, and Lanier LL (2015). Homeostatic control of memory cell progenitors in the natural killer cell lineage. Cell Rep 10, 280–291. [PubMed: 25578733]

Karo JM, Schatz DG, and Sun JC (2014). The RAG recombinase dictates functional heterogeneity and cellular fitness in natural killer cells. Cell 159, 94–107. [PubMed: 25259923]

Kedl RM, Kappler JW, and Marrack P (2003). Epitope dominance, competition and T cell affinity maturation. Curr. Opin. Immunol 15, 120–127. [PubMed: 12495743]

Kedl RM, Rees WA, Hildeman DA, Schaefer B, Mitchell T, Kappler J, and Marrack P (2000). T cells compete for access to antigen-bearing antigen-presenting cells. J. Exp. Med 192, 1105–1113. [PubMed: 11034600]

Kim S, Davis M, Sinn E, Patten P, and Hood L (1981). Antibody diversity: somatic hypermutation of rearranged VH genes. Cell 27, 573–581. [PubMed: 6101208]

Küppers R, Zhao M, Hansmann ML, and Rajewsky K (1993). Tracing B cell development in human germinal centres by molecular analysis of single cells picked from histological sections. EMBO J 12, 4955–4967. [PubMed: 8262038]

Lanier LL (2005). NK cell recognition. Annu. Rev. Immunol 23, 225–274. [PubMed: 15771571]

Lanier LL (2008). Up on the tightrope: natural killer cell activation and inhibition. Nat. Immunol 9, 495–502. [PubMed: 18425106]

Lopez-Vergès S, Milush JM, Schwartz BS, Pando MJ, Jarjoura J, York VA, Houchins JP, Miller S, Kang SM, Norris PJ, et al. (2011). Expansion of a unique CD57^{+} NKG2Chi natural killer cell subset during acute human cytomegalovirus infection. Proc. Natl. Acad. Sci. USA 108, 14725–14732. [PubMed: 21825173]

Love MI, Huber W, and Anders S (2014). Moderated estimation of fold change and dispersion for RNA-seq data with DESeq2. Genome biology 15, 550. [PubMed: 25516281]

MacLennan IC (1994). Germinal centers. Annu. Rev. Immunol 12, 117–139. [PubMed: 8011279]

Madera S, Rapp M, Firth MA, Beilke JN, Lanier LL, and Sun JC (2016). Type I IFN promotes NK cell expansion during viral infection by protecting NK cells against fratricide. J. Exp. Med 213, 225–233. [PubMed: 26755706]

Madera S, and Sun JC (2015). Cutting edge: stage-specific requirement of IL-18 for antiviral NK cell expansion. J. Immunol 194, 1408–1412. [PubMed: 25589075]

Mempel TR, Henrickson SE, and Andrian UHV (2004). T-cell priming by dendritic cells in lymph nodes occurs in three distinct phases. Nature 427, 154–159. [PubMed: 14712275]

Min-Oo G, and Lanier LL (2014). Cytomegalovirus generates long-lived antigen-specific NK cells with diminished bystander activation to heterologous infection. J. Exp. Med 211, 2669–2680. [PubMed: 25422494]

Muccio L, Bertaina A, Falco M, Pende D, Meazza R, Lopez-Botet M, Moretta L, Locatelli F, Moretta A, and Chiesa MD (2016). Analysis of memory-like natural killer cells in human cytomegalovirus-infected children undergoing αβ+T and B cell-depleted hematopoietic stem cell transplantation for hematological malignancies. Haematologica 101, 371–381. [PubMed: 26659918]

Muntasell A, Lopez-Montanes M, Vera A, Heredia G, Romo N, Penafiel J, Moraru M, Vila J, Vilches C, and Lopez-Botet M (2013). NKG2C zygosity influences CD94/NKG2C receptor function and the NK-cell compartment redistribution in response to human cytomegalovirus. European journal of immunology 43, 3268–3278. [PubMed: 24030638]

Muramatsu M, Sankaranand VS, Anant S, Sugai M, Kinoshita K, Davidson NO, and Honjo T (1999). Specific expression of activation-induced cytidine deaminase (AID), a novel member of the RNA-editing deaminase family in germinal center B cells. J. Biol. Chem 274, 18470–18476. [PubMed: 10373455]

Oberle SG, Hanna-El-Daher L, Chennupati V, Enouz S, Scherer S, Prlic M, and Zehn D (2016). A minimum epitope overlap between infections strongly narrows the emerging T cell repertoire. Cell Rep 17, 627–635. [PubMed: 27732840]

Orr MT, Murphy WJ, and Lanier LL (2010). 'Unlicensed' natural killer cells dominate the response to cytomegalovirus infection. Nat. Immunol 11, 321–327. [PubMed: 20190757]

Patro R, Duggal G, Love MI, Irizarry RA, and Kingsford C (2017). Salmon provides fast and bias-aware quantification of transcript expression. Nature methods 14, 417–419. [PubMed: 28263959]

Prlic M, Hernandez-Hoyos G, and Bevan MJ (2006). Duration of the initial TCR stimulus controls the magnitude but not functionality of the CD8+ T cell response. J. Exp. Med 203, 2135–2143. [PubMed: 16908626]

Rahim MM, Wight A, Mahmoud AB, Aguilar OA, Lee SH, Vidal SM, Carlyle JR, and Makrigiannis AP (2016). Expansion and protection by a virus-specific NK cell subset lacking expression of the inhibitory NKR-P1B receptor during murine cytomegalovirus infection. J. Immunol 197, 2325–2337. [PubMed: 27511735]

Soneson C, Love MI, and Robinson MD (2015). Differential analyses for RNA-seq: transcript-level estimates improve gene-level inferences. F1000Research 4, 1521. [PubMed: 26925227]

Strauss-Albee DM, Fukuyama J, Liang EC, Yao Y, Jarrell JA, Drake AL, Kinuthia J, Montgomery RR, John-Stewart G, Holmes S, and Blish CA (2015). Human NK cell repertoire diversity reflects immune experience and correlates with viral susceptibility. Sci Transl Med 7, 297ra115.

Sun JC, Beilke JN, and Lanier LL (2009). Adaptive immune features of natural killer cells. Nature 457, 557–561. [PubMed: 19136945]

Sun JC, Madera S, Bezman NA, Beilke JN, Kaplan MH, and Lanier LL (2012). Proinflammatory cytokine signaling required for the generation of natural killer cell memory. J. Exp. Med 209, 947–954. [PubMed: 22493516]

Trautmann L, Rimbert M, Echasserieau K, Saulquin X, Neveu B, Dechanet J, Cerundolo V, and Bonneville M (2005). Selection of T cell clones expressing high-affinity public TCRs within Human cytomegalovirus-specific CD8 T cell responses. Journal of immunology 175, 6123–6132.

Viant C, Guia S, Hennessy RJ, Rautela J, Pham K, Bernat C, Goh W, Jiao Y, Delconte R, Roger M, et al. (2017). Cell cycle progression dictates the requirement for BCL2 in natural killer cell survival. J. Exp. Med 214, 491–510. [PubMed: 28057804]

Young MD, Wakefield MJ, Smyth GK, and Oshlack A (2010). Gene ontology analysis for RNA-seq: accounting for selection bias. Genome biology 11, R14. [PubMed: 20132535]

Zehn D, Lee SY, and Bevan MJ (2009). Complete but curtailed T-cell response to very low-affinity antigen. Nature 458, 211–214. [PubMed: 19182777]

Highlights:

- Ly49H receptor density drives diversity in NK cell function during MCMV infection
- NK cells undergo avidity selection during CMV infection
- Ly49H^{hi} NK cells possess greater potential for cytotoxic and adaptive responses
- Ly49H^{lo} NK cells possess greater potential for IFN-γ production

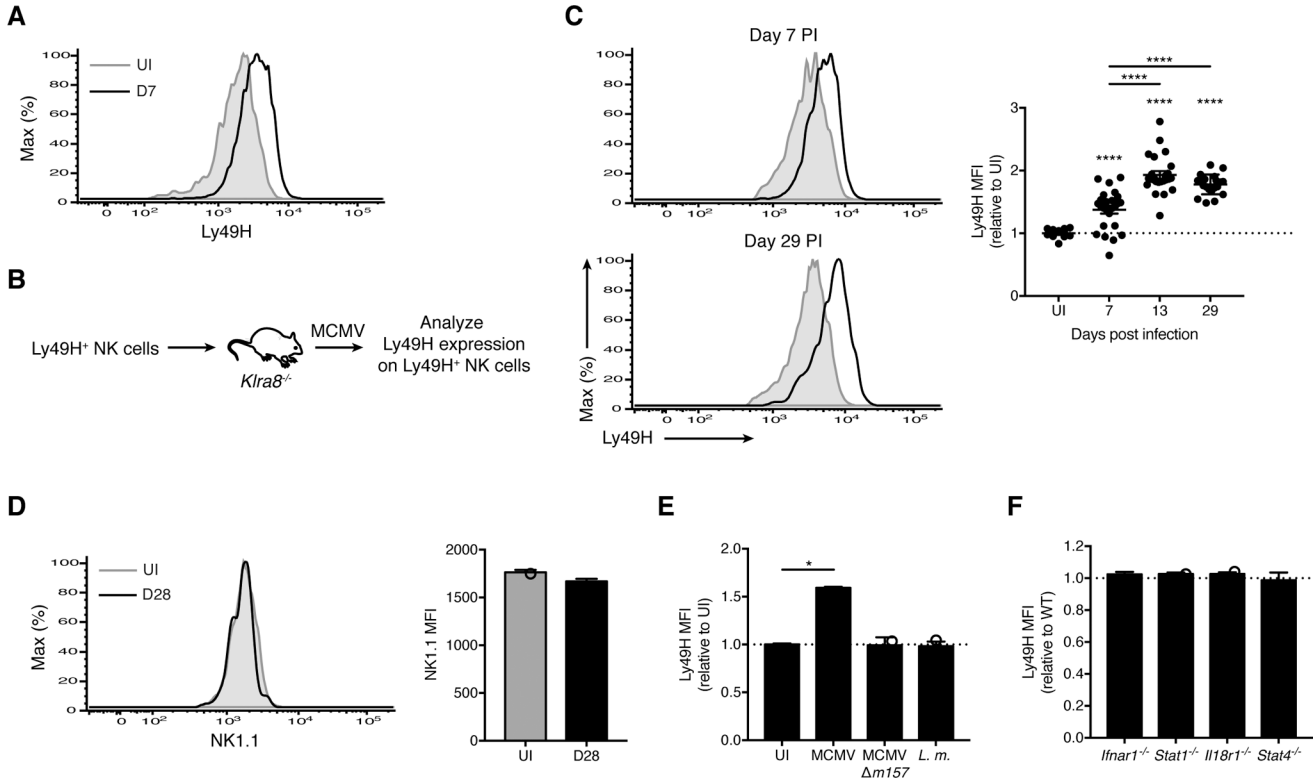

Figure 1. MCMV-driven changes in Ly49H expression within the antiviral NK cell pool are m157-dependent

(**A**) Histograms of Ly49H expression on splenic Ly49H$^+$ NK cells (gating strategy in Figure S1A) from uninfected (UI) and MCMV-infected WT mice at day 7 PI (D7). Data are representative of at least five independent experiments with 5–10 mice per experiment.

(**B-C**) Experimental schematic (B). Ly49H$^+$ NK cells were transferred into *Klra8*$^{-/-}$ mice, and their phenotype analyzed following MCMV infection of the recipients. (C) Histograms of Ly49H expression on Ly49H$^+$ NK cells from blood of UI WT mice (shaded gray) versus at day 7 PI (top left) and day 29 PI (bottom left) (black lines). Quantification of Ly49H median fluorescence intensity (MFI) on Ly49H$^+$ NK cells at indicated days PI relative to UI WT mice bled on the same day (right). Data are representative of three independent experiments with 10–25 mice per experiment.

(**D**) As in (C), histograms (left) and MFI (right) of NK1.1 on Ly49H$^+$ NK cells from blood of UI WT mice and at day 28 PI. Data are representative of at least three independent experiments with 3–9 mice per experiment.

(**E**) WT mice were infected with MCMV, MCMV-*Δm157*, *Listeria monocytogenes* (*L.m.*) or UI. Data is represented as Ly49H MFI on Ly49H$^+$ NK cells from blood at day 7 PI for indicated infections relative to UI. Data are representative of two independent experiments with 2–5 mice per group.

(**F**) As in (B), except splenocytes from WT and indicated knock-out (KO) mice were co-transferred. Data is represented as Ly49H MFI on KO Ly49H$^+$ NK cells relative to WT from blood at day 7 PI. Data are representative of two to four independent experiments with 2–5 mice per group. Groups with a ratio < 1 were compared against 1 using a one sample t test.

Groups were compared using an unpaired, two-tailed Student's t test (D) or against 1 using a one sample t test (E). In (C), each timepoint was compared against 1 using a one sample t test, and against each other using a paired two-tailed t test. Data are presented as the mean ± SEM. *$p < 0.05$; ****$p < 0.0001$. See also Figure S1.

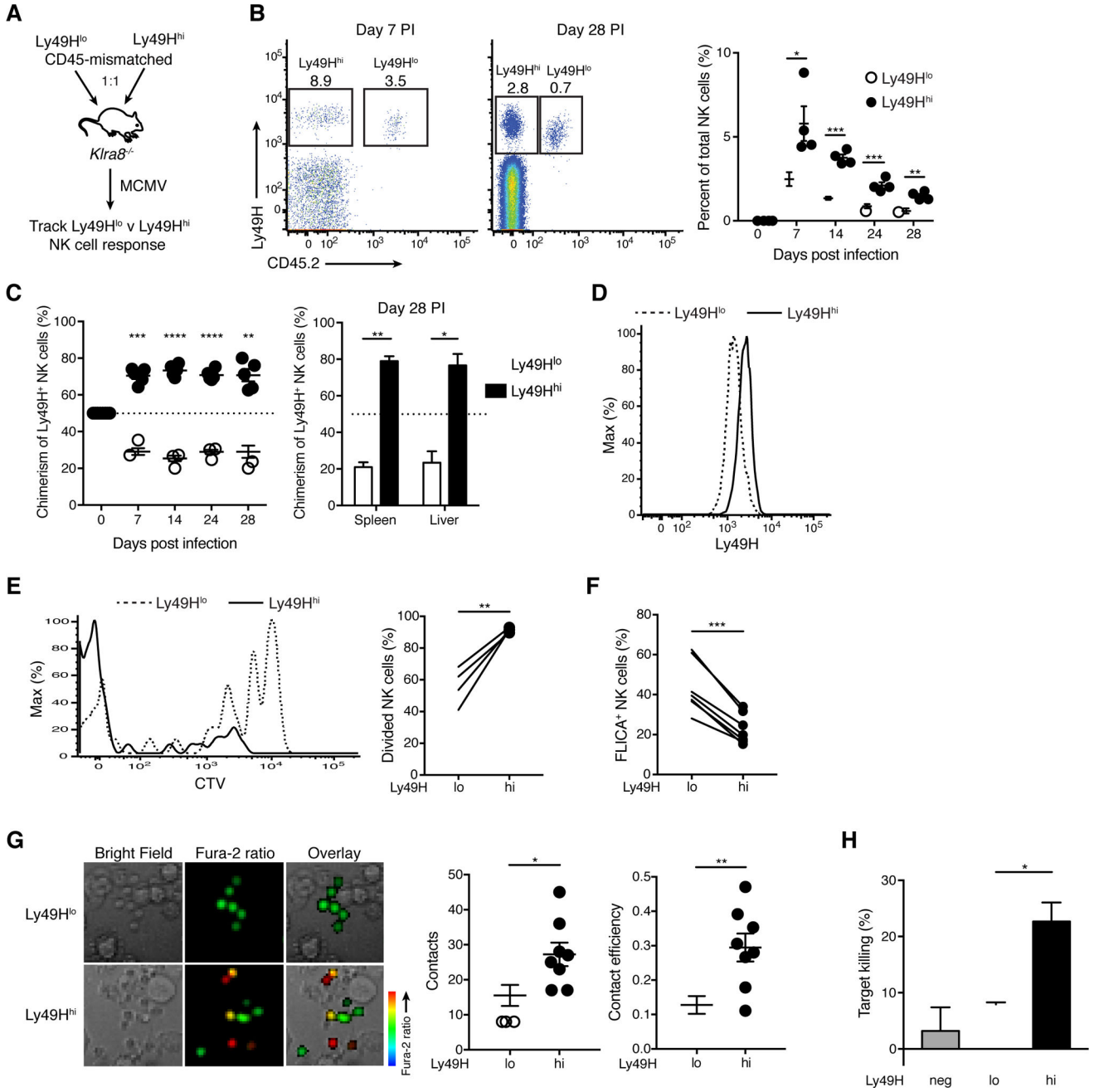

Figure 2. Ly49H^{+} NK cells undergo avidity selection during MCMV infection

(**A-D**) Experimental schematic (A). Equal numbers of splenic Ly49H^{lo} and Ly49H^{hi} NK cells, purified from congenically distinct WT mice, were co-transferred into *Klra8*$^{-/-}$ mice, and their responses tracked following MCMV infection of the recipients. (B) Flow plots gated on NK cells from blood at day 7 PI (left) and spleen at day 28 PI (middle). Quantification of percent Ly49H^{lo} and Ly49H^{hi} NK cells within total NK cells in blood at indicated days PI (right). (C) The percentage of Ly49H^{lo} and Ly49H^{hi} NK cells within transferred Ly49H^{+} NK cells in blood at indicated days PI (left) and in indicated organs at day 28 PI (right). (D) Histograms of Ly49H expression on Ly49H^{lo} and Ly49H^{hi} NK cells

from blood at day 7 PI. Data are representative of two independent experiments with 3–5 mice per experiment.

(**E**) WT splenocytes were labeled with CTV and transferred into congenically distinct WT mice prior to MCMV infection. Histograms of CTV in splenic Ly49H^{lo} and Ly49H^{hi} NK cells at day 7 PI (left). Quantification of indicated NK cell populations that have divided at least once (right). Data are representative of three independent experiments with 4 mice per experiment.

(**F**) Percent of splenic Ly49H^{lo} and Ly49H^{hi} NK cells staining positive for FLICA at day 4 PI. Data are pooled from two independent experiments with 3–4 mice per experiment.

(**G**) Purified splenic Ly49H^{lo} and Ly49H^{hi} NK cells were loaded with Fura-2AM and co-cultured with Ba/F3–m157 cells. Live-cell imaging was then performed. Representative images from the time-lapse analysis (left). Scale bar = 10 μM. Quantification of the number of contacts between NK cells and target cells (middle) and contact efficiency (right), defined as the proportion of target cell contacts that resulted in an NK cell Ca^{2+} flux (change in NK cell color from green to yellow or red). Data are representative of two experiments with 4 replicates per group per experiment.

(**H**) Purified splenic Ly49H^{-}, Ly49H^{lo}, and Ly49H^{hi} NK cells were incubated with Ba/F3–m157 target cells (CTV^{hi}) and Ba/F3 control cells (CTV^{lo}) at 10:1:1 ratio (effector: target: control) for 6 hours. Quantification of target cell killing by indicated NK cell populations compared to control wells lacking NK cells. Data are representative of three independent experiments with 3 replicates per group per experiment. Ly49H^{lo} and Ly49H^{hi} NK cells were compared using an unpaired, two-tailed Student's t test.

Groups were compared using a paired, two-tailed t test (B, E, F), an unpaired, two-tailed Student's t test (G) or against 50 using a one sample t test (C). Data are presented as the mean ± SEM. *p < 0.05, **p < 0.01, ***p < 0.001, ****p < 0.0001. See also Figures S1 and S2.

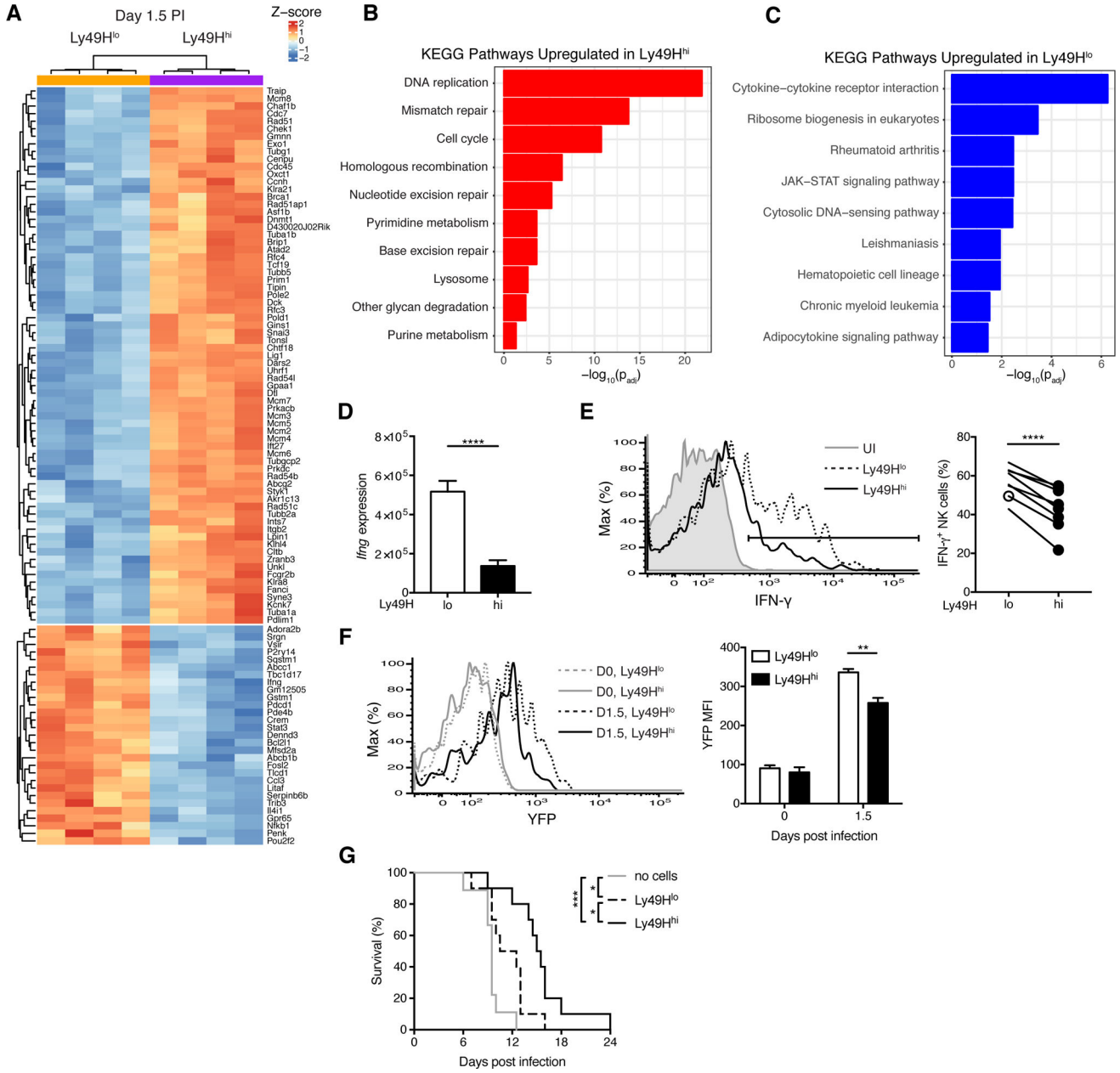

Figure 3. Ly49H^{lo} NK cells produce more IFN-γ during early MCMV infection

(**A-D**) Splenic Ly49H^{lo} and Ly49H^{hi} NK cells were sorted for RNA-seq at day 1.5 PI (4 replicates each). (A) Heat map and hierarchical clustering of top 100 differentially expressed genes by p-value. (B-C) Gene ontology analysis of differential KEGG pathways for genes significantly ($p_{adj} < 0.05$) upregulated in Ly49H^{hi} NK cells (B) and upregulated in Ly49H^{lo} NK cells (C). Their respective p values are shown. (D) Quantification of RNA-seq reads mapping to the *Ifng* locus. P value was calculated in DESeq2 and adjusted for testing multiple hypotheses.

(**E**) Histograms of intracellular IFN-γ expression in splenic Ly49H^{+} NK cells from UI and MCMV-infected WT mice at day 1.5 PI (left). Quantification of percent IFN-γ^{+} NK cells

within indicated NK cell populations (right). Data are representative of at least five independent experiments with 3–15 mice per experiment.

(**F**) As in (E), except UI or MCMV-infected *Ifng*-IRES-YFP mice at day 1.5 PI. Histograms (left) and quantification of YFP MFI (right) before and after MCMV infection. Data are representative of two independent experiments with 2–3 mice per time point per experiment.

(**G**) Kaplan-Meier survival curves of *Rag2*$^{-/-}$ *Il2rg*$^{-/-}$ mice that received either no cells, 50,000 purified Ly49H^{lo} NK cells, or 50,000 purified Ly49H^{hi} NK cells 2 days prior to MCMV infection. Data are pooled from two independent experiments with 4–5 mice per group per experiment.

Groups were compared using a paired, two-tailed t test (E, F) or the Log-rank (Mantel-Cox) test with correction for testing multiple hypotheses (G). Data are presented as the mean ± SEM. *$p < 0.05$, **$p < 0.01$, ***$p < 0.001$, ****$p < 0.0001$. See also Figures S2 and S3 and Table S1.

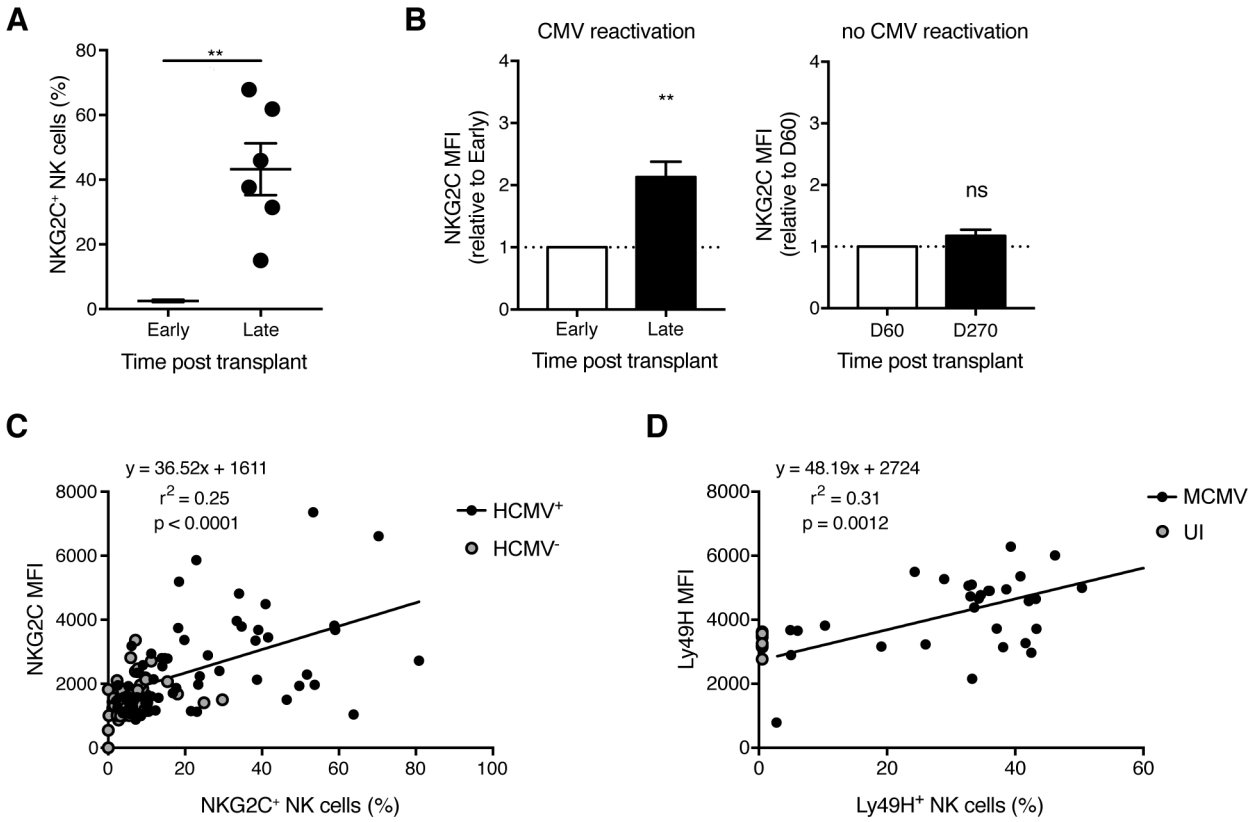

Figure 4. HCMV reactivation in HSCT recipients drives higher NKG2C expression on human NKG2C$^+$ NK cells

(**A-B**) Blood was drawn from T cell-depleted HSCT recipients in the year following transplant (every ~30–90 days). HCMV infection status was determined by viral qPCR. "Early" and "Late" are paired samples from the same HCMV-reactivating transplant recipients. "Early" refers to 15–60 days post transplant depending on the recipient, and "Late" includes the window between 200 days to 1 year post transplant. The data are presented as such to synchronize the timing of adaptive NKG2C$^+$ NK cell appearance, which was recipient-dependent. It was expansion of the NKG2C$^+$ NK cell population that dictated the observed kinetic profile of NKG2C MFI. (A) Percentage of NKG2C$^+$ NK cells among CD3$^-$CD56$^+$ cells (gating strategy in Figure S4). (B) Quantification of NKG2C MFI on NKG2C$^+$ NK cells from transplant recipients who reactivated (left) or did not reactivate (right) HCMV. Groups were compared using a paired, two-tailed t test (A) or against 1 using a one sample t test (B). Data are presented as the mean ± SEM. ns, not significant; **p < 0.01.

(**C**) Blood was drawn from healthy HCMV-seropositive and HCMV-seronegative donors. Correlation between NKG2C MFI and percentage of NKG2C$^+$ NK cells. Linear regression was performed on HCMV$^+$ samples. P value represents the likelihood of a non-zero slope.

(**D**) Experimental design as in Figure 1B. Correlation between Ly49H MFI and the Ly49H$^+$ NK cell expansion (i.e. percentage of Ly49H$^+$ NK cells among total NK cells) at day 7 PI. UI WT mice were assigned 0% expansion. Linear regression was performed on MCMV-infected samples. P value represents the likelihood of a non-zero slope.

See also Figure S4.

KEY RESOURCES TABLE

REAGENT or RESOURCE	SOURCE	IDENTIFIER
Antibodies		
Anti-Mouse CD3ε (clone 17A2)	Tonbo Biosciences	Cat#25–0032; RRID:AB_2621619
Anti-Mouse TCRβ (clone H57–597)	BioLegend	Cat#109220; RRID:AB_893624
Anti-Mouse CD19 (clone 6D5)	BioLegend	Cat#115530; RRID:AB_830707
Anti-Mouse F4/80 (clone BM8.1)	BioLegend	Cat#123117; RRID:AB_893489
Anti-Mouse NK1.1 (clone PK136) for flow cytometry	Tonbo Biosciences	Cat#65–5941; RRID:AB_2621910
Anti-Mouse Ly49H (clone 3D10) for flow cytometry	eBioscience	Cat#11-5886-81; RRID:AB_1257160
Anti-Mouse CD45.1 (clone A20)	BioLegend	Cat#110729; RRID:AB_1134170
Anti-Mouse CD45.2 (clone 104)	BioLegend	Cat#109821; RRID:AB_493730
Anti-Mouse/Human CD11b (clone M1/70)	BioLegend	Cat#101223; RRID:AB_755985
Anti-CD27 (clone LG.7F9)	eBioscience	Cat#14-0271-81; RRID:AB_467182
Anti-Mouse KLRG1 (clone 2F1)	Tonbo Biosciences	Cat#50–5893; RRID:AB_2621800
Anti-Mouse Ly49D (clone 4E5)	BioLegend	Cat#138308; RRID:AB_10639939
Anti-Mouse Ly49C and Ly49I (clone 5E6)	BD Biosciences	Cat#553277; RRID:AB_394751
Anti-Mouse NKG2A/C/E (clone 20D5)	BD Biosciences	Cat#740549; RRID:AB_2740251
Anti-Mouse CD25 (clone PC61)	BioLegend	Cat#102016; RRID:AB_312865
Anti-Mouse IFN gamma (clone XMG1.2)	Tonbo Biosciences	Cat#20–7311; RRID:AB_2621616
Anti-Mouse CD107a (clone 1D4B)	BioLegend	Cat#121611; RRID:AB_1732051
Anti-Stat4 pY693 (clone 38/p-Stat4)	BD Biosciences	Cat#558137; RRID:AB_397052
Anti-Mouse CD218a (IL-18Ra) (clone P3TUNYA)	eBioscience	Cat#48-5183-80; RRID:AB_2574068
Anti-Human CD3 (clone UCHT1)	BD Biosciences	Cat#563852; RRID:AB_2744391
Anti-Human CD56 (clone N901)	Beckman Coulter	Cat#A82943; RRID:AB_2750853
Anti-Human CD159c (NKG2C) (clone REA205)	Miltenyi	Cat#130-117-398; RRID:AB_2727933

REAGENT or RESOURCE	SOURCE	IDENTIFIER
*In Vivo*Mab Anti-Mouse CD8α (clone 2.43) for NK cell enrichment	Bio X Cell	Cat#BE0061; RRID:AB_1125541
*In Vivo*Mab Anti-Mouse CD4 (clone GK1.5) for NK cell enrichment	Bio X Cell	Cat#BE0003–1; RRID:AB_1107636
*In Vivo*Mab Anti-Mouse CD19 (clone 1D3) for NK cell enrichment	Bio X Cell	Cat#BE0150; RRID:AB_10949187
*In Vivo*Mab Anti-Mouse Ter-119 (clone TER-119) for NK cell enrichment	Bio X Cell	Cat#BE0183; RRID:AB_10949625
LEAF™ Purified Anti-Mouse NK-1.1 (clone PK136) for plate-bound stimulation	BioLegend	Cat#108712; RRID:AB_ 313399
LEAF™ Purified Anti-Mouse Ly49H (clone 3D10) for plate-bound stimulation	BioLegend	Cat#144704; RRID:AB_ 2561551
Bacterial and Virus Strains		
Mouse Cytomegalovirus (MCMV)	J. Sun (PI)	Smith Strain
MCMV-Δm157	U. Koszinowski (PI) (Bubić et al., 2004)	N/A
Listeria monocytogenes	J. Sun (PI)	N/A
Biological Samples		
Healthy human donor buffy coats	New York Blood Center	http://nybloodcenter.org/
Chemicals, Peptides, and Recombinant Proteins		
Recombinant Mouse IL-12 Protein	R&D Sytems	Cat#419-ML
Recombinant Mouse IL-18	MBL	Cat#B002–5
Phorbol 12-myristate 13-acetate (PMA)	Sigma-Aldrich	Cat#P8139
Ionomycin calcium salt from *Streptomyces conglobatus* (Ionomycin)	Sigma-Aldrich	Cat#I0634
Critical Commercial Assays		
TRIzol™ Reagent	Thermo Fisher Scientific	Cat#15596026
eBioscience™ Foxp3 / Transcription Factor Staining Buffer Set	Thermo Fisher Scientific	Cat#00-5523-00
BioMag Goat Anti-Rat IgG (NK cell enrichment)	Qiagen	Cat#310107

REAGENT or RESOURCE	SOURCE	IDENTIFIER
CellTrace™ Violet Cell Proliferation Kit	Thermo Fisher Scientific	Cat#C34557
FAM FLICA™ Poly Caspase Kit	Bio-Rad	Cat#ICT092
Fura-2, AM, cell permeant	Thermo Fisher Scientific	Cat#F1201
eBioscience™ Fixable Viability Dye eFluor™ 506	eBioscience	Cat#65-0866-14
LIVE/DEAD™ Fixable Aqua Dead Cell Stain Kit, for 405 nm excitation	Thermo Fisher Scientific	Cat#L34966
Deposited Data		
Raw Data Files for RNA Sequencing (Ly49H^{lo} versus Ly49H^{hi})	NCBI Gene Expression Omnibus	GSE129490
Experimental Models: Cell Lines		
Mouse: Ba/F3 cells	L. Lanier (PI)	N/A
Mouse: Ba/F3–m157 cells	L. Lanier (PI) (Arase et al., 2002)	Derived from parental Ba/F3 cells
Experimental Models: Organisms/Strains		
Mouse: WT or CD45.2: C57BL/6J	The Jackson Laboratory	Stock#000644; RRID:IMSR_JAX:000664
Mouse: WT or CD45.1: B6.SJL-*Ptprc*^{a} *Pepc*^{b}/BoyJ	The Jackson Laboratory	Stock#002014; RRID:IMSR_JAX:002014
Mouse: *Klra8*$^{-/-}$ or Ly49H-deficient	S. Vidal (PI) (Fodil-Cornu et al., 2008)	N/A
Mouse: *Stat4*$^{-/-}$, *Ifnar1*$^{-/-}$, *Stat1*$^{-/-}$, *Il18r1*$^{-/-}$	J. Sun (PI)	N/A
Mouse: *Ifng*-IRES-YFP or GREAT: B6.129S4-*Ifng*$^{tm3.1Lky}$/J	The Jackson Laboratory	Stock#017581; RRID:IMSR_ JAX:017581
Mouse: *Rag2*$^{-/-}$ *IL2rg*$^{-/-}$: C;129S4-*Rag2*$^{tm1.1Flv}$ *Il2rg*$^{tm1.1Flv}$/J	The Jackson Laboratory	Stock#014593; RRID:IMSR_JAX:014593
Software and Algorithms		
Trimmomatic (v.0.36)	Bolger et al., 2014	http://www.usadellab.org/cms/?page=trimmomatic
Salmon (v0.10.2)	Patro et al., 2017	https://combine-lab.github.io/salmon
tximport (v1.9.12)	Soneson et al., 2015	https://bioconductor.org/packages/release/bioc/html/tximport.html
DESeq2 (v.1.12.17)	Love et al., 2014	http://bioconductor.org/packages/release/bioc/html/DESeq2.html
goseq (v1.33.0)	Young et al., 2010	https://bioconductor.org/packages/release/bioc/html/goseq.html
KEGG.db (v3.2.3)	https://bioconductor.org/packages/release/data/annotation/html/KEGG.db.html	https://bioconductor.org/packages/release/data/annotation/html/KEGG.db.html

REAGENT or RESOURCE	SOURCE	IDENTIFIER
R (v.3.5.1)	https://www.r-project.org/	https://www.r-project.org/
SlideBook software (v6.0.15)	Intelligent Imaging Innovations	https://www.intelligent-imaging.com/slidebook